Polyhedron 124 (2017) 166–176

Contents lists available at ScienceDirect

Polyhedron

journal homepage: www.elsevier.com/locate/poly

Geometric and electronic properties in a series of phosphorescent heteroleptic Cu(I) complexes: Crystallographic and computational studies

Katharina Kubiček [a,b,*], Sreevidya Thekku Veedu [a,b], Darina Storozhuk [a,b], Reza Kia [a,b,*,1], Simone Techert [a,b,c,*]

[a] FS-SCS, Deutsches Elektronen-Synchrotron (DESY), Notkestraße 85, 22607 Hamburg, Germany
[b] Max Planck Institute for Biophysical Chemistry, Am Fassberg 11, 37077 Göttingen, Germany
[c] Institute of X-ray Physics, Göttingen University, Friedrich-Hund-Platz 1, 37077 Göttingen, Germany

ARTICLE INFO

Article history:
Received 23 August 2016
Accepted 18 December 2016
Available online 31 December 2016

Keywords:
Bisphosphines
Copper(I)
Density functional
Crystal structure
Excited state

ABSTRACT

We have investigated the electronic and geometric structures in the lowest excited states of six phosphorescent heteroleptic $[Cu^{I}(NN)(DPEphos)]^{+}$ (DPEphos = bis[(2-diphenylphosphino)phenyl]ether) complexes with varying NN = diimine ligand structures using density functional theory. In comparison to the ground state, the results show a decrease of the dihedral angle between the N–Cu–N and P–Cu–P planes for these excited states with mixed ligand-to-ligand (DPEphos lone pair → π^*(NN)) and metal-to-ligand charge transfer (dπ(Cu) → π^*(NN)) character. Sterically less demanding ligands facilitate this process, which is accompanied by a geometric relaxation of the DPEphos ligand and contraction of the Cu–N bonds. The density functional for the excited state calculations has been selected based on ground state validation studies. We evaluated the ability of seven density functionals to reproduce the molecular ground state geometries and absorption spectra obtained by single-crystal X-ray diffraction and solution-phase UV–Vis absorption spectroscopy respectively. Standard methods (PBE and B3LYP), which do not account for dispersion, systematically overestimate internuclear distances. In contrast, approaches including dispersion (B97D3, PBE0-GD3, M06L, M06, ωB97XD) remove this systematic effect and give less expanded molecular structures. We found that only the hybrid functionals (B3LYP, PBE0-GD3, M06), incorporating a portion of exact exchange from Hartree–Fock theory, accurately predict the experimental absorption energies.

1. Introduction

Transition metal coordination complexes often show advantageous properties, such as a strong visible ground state absorption and excited state emission for their application in dye-sensitized solar cells [1,2], chemo- and biosensors [3–5] as well as organic light emitting diodes (OLED-s) [6,7]. Consequently, the design and synthesis of transition metal complexes has become a more and more active field of research [8,9]. As 4d and 5d metals are relatively expensive and not abundant, 3d transition metal compounds and in particular d^{10} Cu(I) based complexes have been discussed as alternatives [10–14]. It is important to note that for such complexes, excited state characteristics such as lifetimes and luminescence quantum yields are extremely sensitive to variations in their respective ligand structure [15], which in principle allows tuning for applications [16,17]. However, a detailed understanding of universal correlations between ground and excited state properties of the complexes is necessary for the development of more efficient sensitizers and phosphorescent materials [18–20].

Therefore, numerous density functional theory (DFT) calculations and experiments have investigated the excited states of homoleptic prototype $[Cu(NN)_2]^{+}$ complexes with two diimine ligands (NN), in particular $[Cu(dmp)_2]^{+}$ (dmp = 2,9-dimethyl-1,10-phenanthroline) [21–40]. The results indicate that photoexcitation of these complexes leads to a singlet metal-to-ligand charge transfer (^{1}MLCT) excited state and a subsequent ligand-dependent decrease in the dihedral angle (dha) between the NN ligand planes

* Corresponding authors at: FS-SCS, Deutsches Elektronen-Synchrotron (DESY), Notkestraße 85, 22607 Hamburg, Germany.
E-mail addresses: katharina.kubicek@desy.de (K. Kubiček), rkia@sharif.edu (R. Kia), simone.techert@desy.de (S. Techert).
[1] Present address: Chemistry Department, Sharif University of Technology, P.O. Box 11155-3516, Tehran, Iran.

http://dx.doi.org/10.1016/j.poly.2016.12.035
0277-5387/

in the excited states. The geometry change is accompanied by an increase in the non-radiative decay, in particular for the energetically lowest triplet charge transfer (^{3}CT) state after intersystem crossing [21–35]. Those findings have stimulated the design and synthesis of Cu(I) complexes with more constraining ligands, which may hamper a ligand torsional motion and improve the excited state characteristics for applications. For systems with the phen* ligand (phen* = 1,10-phenanthroline derivate), substituents in the 2,9-positions of the phen* unit were found to be most effective [11,41,42]. Moreover, heteroleptic complexes with more bulky ligands show extraordinary properties. Extreme examples are $[Cu(NN)(PP)]^+$ (PP = diphosphine) and in particular $[Cu(phen^*)(DPEphos)]^+$ (DPEphos = bis[(2-diphenylphosphino)phenyl] ether) complexes [17,43–50]. In comparison to analogous homoleptic complexes, the radiative lifetimes and luminescence quantum yields of their lowest excited states are enhanced by orders of magnitude and the complexes have been already successfully tested for OLED and light-emitting electrochemical cell applications [17,43–50]. Also for this class of compounds, a minor variation in the substituent of the 1,10-phenanthroline (phen) moiety, in particular at the 2,9-positions, can change the excited state parameters by factors of up to one hundred [43,44].

Based on this information, it is important to study the electronic and geometric structures of heteroleptic $[Cu(phen^*)(DPEphos)]^+$ complexes in their excited states, in particular for different substituents at the phen unit. For $[Cu(phen^*)(DPEphos)]^+$ or related complexes, so far the corresponding work [48–52], and in particular also quantum chemical computations, are comparatively sparse, but such calculations are the first important step in the investigations of excited states [106]. They provide the background for further (spectroscopic) studies and can complement and support the interpretation and analysis of experimental data. This requires, however, a reliable and accurate computation of molecular structures, in particular, as the results from geometry optimizations can dramatically influence subsequent calculations, e.g. determinations of absolute energies [53,54].

Nowadays, DFT is the most advanced theory which can be used to calculate the electronic and geometric structures of $[Cu(phen^*)(DPEphos)]^+$ complexes. Nevertheless, DFT still faces a number of challenges, which may lead to less accurate results [55–58]. Validation studies have shown that the calculated geometric and electronic parameters can dramatically depend on the choice of the density functional and for each type of calculation some functionals are more fitting than others [53,54,59–70]. Moreover, for any given property and molecular system, suitable functionals can be different and it is highly advisable to first perform benchmark studies for the respective target system [53,54,59–70]. For the $[Cu(phen^*)(DPEphos)]^+$ complexes, the relative positioning of the large phen* and DPEphos ligands, and thus the geometry of the molecule, will be affected by dispersion, which is not included in standard DFT approaches [71,72]. Moreover, the calculated absorption spectra and highest occupied molecular orbital (HOMO) to lowest unoccupied molecular orbital (LUMO) energy gaps are expected to depend significantly on the treatment of the exchange part of the energy in the DFT calculations [54]. In this context, ground state validation studies are important as they can evaluate the ability of functionals to accurately predict the structures of $[Cu(phen^*)(DPEphos)]^+$ complexes. Based on these studies, an appropriate functional can be selected and then be used in subsequent calculations, in particular for the excited states. For validation, usually the results from DFT are compared to a reference, and for the $[Cu(phen^*)(DPEphos)]^+$ complexes ground state structures from X-ray diffraction (XRD) and experimental absorption spectra are the only available standard for evaluation [44,45,48–50,73]. DFT geometry optimizations, however, are usually done on single molecules, while XRD measurements are performed on single-crystals. In contrast to single molecules, the structure of molecules in crystals is influenced by surrounding molecules. Consequently, a comparison of the structures as calculated by DFT and measured by XRD suffers from intrinsic uncertainties. The magnitude of this uncertainty needs to be estimated in order to identify when a deviation between molecular structures from DFT and XRD may originate simply from crystal packing effects and is not significant for validation.

In this paper, we present both experimental and theoretical studies of six phosphorescent heteroleptic $[Cu(NN)(DPEphos)]^+$ complexes (**1**–**6**) (Fig. 1) with varying NN ligand structures. We have investigated the electronic and geometric structures of the complexes in their lowest excited states using DFT. To obtain accurate results, the density functional for the excited state calculations has been selected based on ground state validation studies. We evaluated the ability of seven density functionals to reproduce the ground state molecular structures and absorption spectra derived from single-crystal XRD and solution-phase UV–Vis absorption spectroscopy respectively, both from our own experiments as well as from previously reported measurements by other groups [44,45,48–50,73,74]. Both functionals not considering dispersion as well asaccounting for dispersion were tested. The magnitude of the uncertainty in those validation studies due to crystal packing effects was estimated in an approximate fashion. We determined the influence of surrounding molecules on the structure of molecules in single-crystals by comparing the molecular structures of complexes **1**, **2** and **6** in different crystalline environments, using both data from own XRD measurements and from previously published experiments by other groups [44,48–50,74].

2. Materials and methods

2.1. Selection of the $[Cu(NN)(DPEphos)]^+$ complexes

Compounds **1**–**5** were selected to be representative of the family of $[Cu(phen^*)(DPEphos)]^+$ complexes with systematic variations in their phen* substituent structure, in particular for the prominent 2,9-positions (**1**–**4**). An additional criterion was the availability of their ground state crystal structures as a reference for density functional validation (**1**–**5**; Cambridge Structural Database [44,45,48–50,73,75]). To complement the studies, the influence of a substantial chemical variation of the NN ligand structure was investigated for complex **6** [74]. Complexes **1**, **2** and **6** were chosen for our XRD measurements and a representative comparison of molecular structures in different crystal environments.

2.2. Synthesis and chemical analysis

All reagents were purchased from Aldrich and used as received. Solvents were spectral grade. $[Cu(phen)(DPEphos)]BF_4$ (**1**), $[Cu(dmp)(DPEphos)]BF_4$ (**2**) and $[Cu(bq)(DPEphos)]PF_6$ (**6**) were synthesized according to the reported literature procedures [43,44,48–50,50,74]. The products were analyzed by Electrospray Ionization Mass Spectrometry (ESI-MS, Varian MS-500), Fourier-transform infrared spectroscopy (FT-IR, Bruker IFD 25) and ^{1}H nuclear magnetic resonance spectroscopy (NMR, Agilent Oxford 400 MHz), confirming the successful synthesis of complexes **1**, **2** and **6**. Details can be found in the Appendix A, Supplementary data (SD).

2.3. Single crystal X-ray diffraction

Single crystals of complexes **1**, **2** and **6** suitable for XRD analysis were grown from a solution of the synthesized powders in methanol, acetonitrile and dichloromethane (DCM) respectively by slow

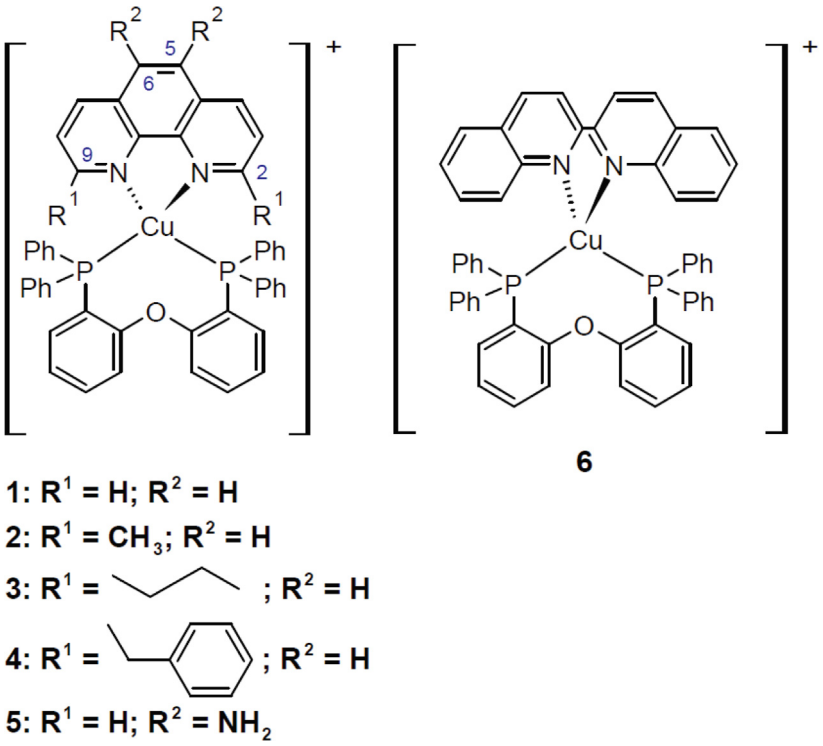

Fig. 1. Schematic structures of the heteroleptic Cu(I) compounds of the type $[Cu(NN)(DPEphos)]^+$ studied within this work. DPEphos = bis[(2-diphenylphosphino)phenyl] ether, Ph = phenyl. R^1 = H, R^2 = H, $[Cu(phen)(DPEphos)]^+$ (**1**); R^1 = methyl, R^2 = H, $[Cu(dmp)(DPEphos)]^+$ (**2**); R^1 = *n*-butyl, R^2 = H, $[Cu(dbp)(DPEphos)]^+$ (**3**); R^1 = phenethyl, R^2 = H, $[Cu(dpep)(DPEphos)]^+$ (**4**); R^1 = H, R^2 = NH_2, $[Cu(dap)(DPEphos)]^+$ (**5**); $[Cu(bq)(DPEphos)]^+$ (**6**). Ligands are phen = 1,10-phenanthroline, dmp = 2,9-dimethyl-1,10-phenanthroline, dbp = 2,9-di-*n*-butyl-1,10-phenthroline, dpep = 2,9-diphenethyl-1,10-phenanthroline, dap = 5,6-diamino-1,10-phenanthroline and bq = 2,2′-biquinoline.

evaporation of the solvent. For complexes **1** and **6**, the crystals were found to be unstable under ambient conditions, while crystals of complex **2** were observed to be stable. The crystallographic experiments were performed on a Bruker SMART APEX II system based on a D8 three-circle diffractometer with an Incotac microfocus X-ray source. The X-ray diffraction data were collected using graphite-monochromated and 0.5 mm-MonoCap-collimated Mo Kα radiation (λ = 0.71073 Å) at 100 K with an Oxford Cryojet low-temperature cooling device. Details on data integration and refinement can be found in Ref. [76] and the SD.

2.4. Photophysical measurements

A CARY 5E spectrophotometer was utilized to measure the electronic absorption spectra of complexes **1**, **2** and **6** in DCM. Similar to the work by Hallmann et al. [77], electronic emission spectra in DCM were recorded with a Horiba Fluorolog spectrophotometer. Complexes **1** and **2** were excited at 400 nm and complex **6** at 450 nm while recording emissions in the wavelength region 500–800 nm.

2.5. Theoretical calculations

All calculations were performed for the cations of complexes **1**–**6** (Fig. 1) and used the GAUSSIAN09 (G09) [78] program with the DFT method. Density functionals for the calculation of the singlet ground state structures of **1**–**6** spanned from the standard GGA functional PBE [79] and the hybrid-GGA functional B3LYP [80,81], which do not account for dispersion to functionals which consider dispersion. The latter include the GGA functional B97D3 [82,107], the hybrid-GGA PBE0 with the GD3 correction [79,83,84], the hybrid-meta-GGA ωB97XD [85,86], which also includes long-range corrections as well as semi-empirical functionals, the local meta-GGA M06L and hybrid-meta M06 [87,88]. The latter include non-covalent interactions and were constructed with dispersive interactions in mind using parameters from extensive validation studies [87,88]. In all the calculations, the Stuttgart-Dresden (SDD) [89] basis set and effective core potential (ECP) were utilized for the Cu atom and the 6-31G* basis set was used for all other atoms. For the description of the complexes in solution we used the conductor-like polarizable continuum model (CPCM) [91–93] with DCM as a solvent. The structures of the singlet ground and lowest lying triplet excited states were optimized to their lowest minimum energy point on their potential energy surfaces and a full analysis of the molecular orbitals (MO-s) was performed. Based on the ground state validation studies, the PBE0-GD3 functional was selected for calculations on triplet excited states. These calculations use the unrestricted wave function formalism and were carefully checked for spin contamination. The stability of all geometries was tested by a frequency analysis. TD-DFT calculations [90] of the vertical excitation, at the singlet ground state equilibrium geometry, with linear response, non-equilibrium solvation provided 40 singlet and triplet transition energies as well as their corresponding oscillator strengths and character upon electronic ground state excitation. For complex **2**, the relaxation of the singlet excited state geometry after vertical excitation was investigated by TD-DFT geometry optimizations with equilibrium, linear response solvation providing the minimum energy point on the excited state potential energy surface. To break the symmetry at the start of the optimization, ground state geometries were perturbed slightly changing the dihedral angle (dha) between the N–Cu–N and P–Cu–P planes. For the generation of (partial) density of states (PDOS) and to display the electronic spectra GaussSum 2.2 [94] was utilized. For molecular graphics, the

programs MERCURY [95], Avogadro [96] and ChemCraft [97] were employed.

2.6. Comparison of the structures

Following the approach by Minenkov et al. [53], we investigated deviations between geometries for two structures by evaluating the mean signed error (MSE) and mean unsigned error (MUE) for changes in all interatomic distances and in bonding distances to the Cu(I) coordination center respectively. The MSE and MUE were calculated according to MSE = 2/(N(N-1)) * Σ_i^N-1Σ_j > i^N (|Rij (DFT)-Rij(X-ray)|) and MUE = 2/(N(N-1)) * Σ_i^N-1Σ_j > i^N (Rij (DFT)-Rij(X-ray)) [53]. Here, Rij is the interatomic distance between atoms i and j and N is the number of atoms. This approach allows the study of systematic variations in bond lengths that are not easy to access by a simple comparison of molecular Cartesian coordinates [53]. Large distances which are influenced by Van der Waals interactions dominate the MSE and MUE for the all distances approach [53] and a corresponding evaluation tests the ability of the density functionals to describe those interactions. For details see Ref. [53] and the SD.

3. Results and discussion

3.1. Molecular ground state structures from X-ray crystallography

To estimate the deviations in molecular structural parameters for different crystal packing, MSE and MUE-s for changes in the interatomic distances of the molecular structures of complexes **1**, **2** and **6** were calculated, comparing results from our XRD experiments and previously reported crystallographic measurements for the complexes by other research groups [44,48–50,74]. For a maximum variation in crystal packing, in comparison to previous crystallization processes [44,48–50,74], we utilized different solvents and counterions. Consequently, we observed significant differences in the crystal systems, space groups, asymmetric unit and unit cell structural parameters (SD). Key crystallographic data from our measurements are presented in Table 1.

In Fig. 2 we have superposed the molecular structures for complex **1** as derived by XRD within this work and by Kuang et al. [44]. The corresponding figures for complexes **2** and **6** are presented in the SD. Results by Zhang et al. [50] and Yang et al. [49] on one hand and Costa et al. [48] on the other hand are similar to the results by Kuang et al. [44] and our results respectively, and thus are omitted here. Both common motifs and significant structural differences are found. All the XRD experiments for complexes **1**, **2** and **6** show that the Cu(I) center is in a distorted tetrahedral coordination environment and that the NN ligand is tilted towards one of the two P atoms. Also, the O atom of the DPEphos ligand is at a non-bonding distance (>3.0 Å) and for complex **1** we found an intramolecular π-stacking interaction between the phen ligand and a phenyl group of the DPEphos ligand, which has been previously reported by Costa et al. [48]. The dha-s between the average N–Cu–N and P–Cu–P planes are nearly identical for the two different crystal structures of complex **1** and **2**, ~89° and ~82° respectively, but for complex **6** a difference of 6° is observed (this work: 88.6°; 82.6° [74]). Furthermore, in comparison to Refs. [44,49,50,74], we found displacements, rotations and tiltings of the phenyl groups of the DPEphos ligand as well as tiltings of the average Cu-phen (**1**) or Cu-bq (**6**) planes nearly perpendicular to the P–Cu–P plane by angles of around 7° and 32° respectively (Fig. 2 and SD). An analysis, including all interatomic distances of the three complexes, reveals that those differences in molecular structures correspond to an average MSE of ~0.025 Å and MUE of ~0.25 Å (Fig. 3, upper graph, "crystal packing"). In other words, the average change in interatomic distance for the same molecule in a different crystal lattice is of the order of ~0.025 Å and the absolute value of all changes in distances is ~0.25 Å.

In Table A1 (SD) we compare important bond lengths (Å) and valence angles (°) of complexes **1**, **2** and **6**, as derived by XRD within this work (Exp.) and by Kuang et al. [44] and Zhang et al. [74] respectively. An analysis including all the valence angles at the Cu atom of the three complexes gives an average standard deviation of ~2° for differences in the valence angles between two different structures of the same complex. An evaluation of all the Cu–N and Cu–P bond lengths of the three complexes provides an average MSE of ~0.01 Å and MUE of ~0.02 Å (Fig. 3, lower graph, "crystal packing"). Both the standard deviation of the valence angles and the MSE are of the order of the typical standard deviations of 1–2° or 0.01–0.02 Å respectively reported by Martin et al. [98] for a variety of transition metal complexes in different crystal environments.

3.2. Ground state geometric structures: X-ray crystallography and density functional theory

The ground state structures of complexes **1**–**6** have been calculated using seven different density functionals and the calculated structures have been compared to molecular ground state geometries derived from XRD experiments, using both data from own measurements and previously published results from other research groups [44,45,48–50,73,74]. The MSE-s and MUE-s for an analysis including all the interatomic distances of complexes **1**–**4** and **6** are shown in Fig. 3 (upper graph). In addition, the lower part of Fig. 3 depicts the MSE-s and MUE-s for an evaluation of all the Cu–N and Cu–P bond lengths of the complexes. Complex **5** is excluded in this analysis as our calculations indicate that the molecular structure of this complex, as measured by XRD, does not correspond to the calculated structure for its ground state (for more details refer to the following sections). Fig. 3 shows that the standard functionals B3LYP and PBE substantially overestimate the interatomic distances and predict expanded molecular structures, providing MSE-s of 0.1–0.15 Å for the all interatomic distances method. For the functionals which consider dispersion, B97D3, PBE0G-D3, M06L, M06 and ωB97XD, the MSE-s nearly vanish (<0.05 Å), indicating that the overestimation of bond distances is compensated, and similar results have been reported for the molecular structures of ruthenium complexes [53]. It should be noted here that the average change in an interatomic distance for the same molecule in a different crystal lattice is ~0.025 Å ("crystal lattice", Fig. 3, upper graph), and thus substantially smaller than the differences between MSE-s derived for the different groups of density functionals, i.e. MSE-s are a reliable quantity for density functional validation. An evaluation of the MUE-s shows that functionals which consider dispersion give on average lower absolute errors, MUE-s <0.020 Å, than functionals not accounting for dispersion, MUE-s >0.022 Å. However, MUE-s for differences in all interatomic distances of the same molecule in different crystal environments ("crystal lattice", Fig. 3, upper graph) show average uncertainties of up to ~0.25 Å, i.e. the MUE-s are not a reliable quantity for validation. An analogous comparison of bonding distances to the Cu coordination center (Fig. 3, lower graph) indicates that the B3LYP functional clearly overestimates the metal–ligand bond lengths. In agreement with previous reports for transition metal complexes [53] the standard PBE functional predicts bond lengths for the Cu center much more accurately, but as discussed above is not well suited to calculate accurate overall geometries for the molecules.

A qualitative comparison of the ground state structures as measured by XRD and calculated by DFT for the different functionals supports the finding that functionals which account for dispersion

Table 1
Crystallographic data for [Cu(phen)(DPEphos)]BF_4·CH_3OH·0.36 H_2O (**1**), [Cu(dmp)(DPEphos)]BF_4·CH_3CN (**2**) and [Cu(bq)(DPEphos)]PF_6·0.5·CH_2Cl_2·0.2 H_2O (**6**).

Complex	**1**	**2**	**6**
Empirical formula	$C_{49}H_{40.72}BCuF_4N_2O_{2.36}P_2$	$C_{52}H_{43}BCuF_4N_3OP_2$	$C_{54.5}H_{41.4}ClCuF_6N_2O_{1.2}P_3$
Formula mass	907.7	938.18	1049.39
Crystal system	monoclinic	monoclinic	triclinic
Color	yellow	yellow	orange
Space group	$P2_1/n$	$P2_1/c$	$P\bar{1}$
a (Å)	12.8059(16)	10.7644(4)	12.7211(5)
b (Å)	25.266(3)	14.4216(6)	13.2166(5)
c (Å)	13.5370(17)	28.8783(12)	15.2889(6)
α (°)	90	90	80.459(2)
β (°)	103.874(2)	98.410(2)	88.870(2)
γ (°)	90	90	66.621(2)
V (Å3)	4252.2(9)	4434.9(3)	2323.83(16)
Z	4	4	2
ρ_{calc} (g/cm^3)	1.418	1.405	1.500
$F(000)$	1873.5	1936.0	1074.0
μ (mm^{-1})	0.651	0.625	0.700
Data/restraints/parameters	9389/42/711	12449/0/580	11073/0/643
Reflections collected	74323	182701	44055
Goodness-of-Fit (GOF) on F^2	1.054	1.045	1.042
2Θ range for data collection (°)	3.224 to 54.214	2.852 to 59.336	2.704 to 55.754
R_{int}	0.0747	0.1669	0.0485
R_1 [I > 2sigma(I)]	0.0538	0.0550	0.0482
wR_2 [I > 2sigma(I)]	0.1420	0.1405	0.1084
R_1 (all data)	0.0688	0.0772	0.0693
wR_2 (all data)	0.1506	0.1482	0.1185
Residuals (e Å^{-3})	0.55/−0.46	1.16/−1.17	0.65/−0.59

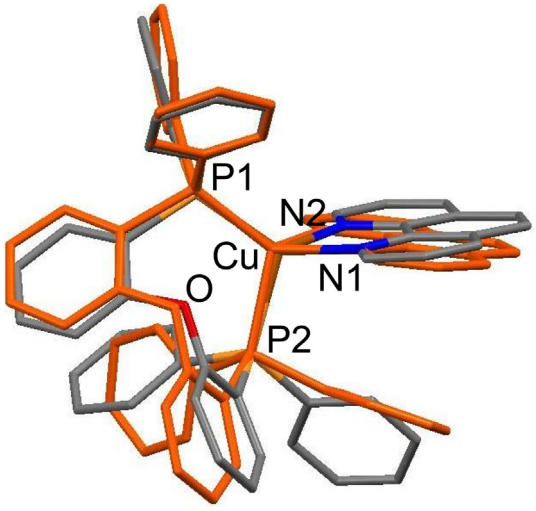

Fig. 2. Superposition of the molecular ground state structure of complex **1** determined by crystallography within this work (orange) and by Kuang et al. (element-colored) [44]. Our results show a disorder of the phen ligand (two positions with occupancy of 75:25; CCDC 1498327) for the asymmetric unit and here, for better comparison, we only show one of the two molecular structures. (Color online.)

offer an improved description of the ground state molecular structures and this is depicted in Fig. 4 for complex **1**. In particular, for the phen moiety the PBE0-GD3 functional reproduces the experimental structure more closely.

Based on the validation studies, for a further analysis we have selected calculations at the PBE0-GD3 level. In Table 2 we present the corresponding bond lengths and valence angles for the Cu coordination center. An evaluation of the dha-s between the average N–Cu–N and the P–Cu–P planes for complexes **1**–**4** and **6** gives good agreement between the experimentally measured and calculated values, 88.9°/84.8° (**1**), 82.4°/82.5° (**2**), 78.8°[44]/79.9°(**3**), 86.7°[45]/88.4° (**4**) and 88.6°/89.3° (**6**), respectively. The dha-s in the ground state of complexes **2** and **3** are substantially smaller than for complexes **1**, **4** and **6**. In other words, complexes **2** and **3** show a larger geometrical distortion in their ground state and in particular a decrease in the dha is observed for an increase in the alkyl chain length of the substituent at the 2,9-position of the phen* unit. This distortion is accompanied by a tilting of the phen* unit in direction of one of the P atoms of the DPEphos ligand (SD) and results in an angle of ~11° between the Cu–NN and N–Cu–N planes for complexes **2** and **3**. In contrast, these angles are around 0–3° for complexes **1** and **4**. It should be noted that for complex **4** with a bulky phenethyl ligand in the 2,9-position, in principle, a substantial distortion in the dha for the ground state is expected. However, our calculations show that an intramolecular π-stacking interaction between a phenyl unit of the phenethyl ligand and one phenyl moiety of the DPEphos ligand effectively constrains the dihedral angle of the molecule to close to around 88°. In addition, we want to mention here that a comparison of ground state structures derived from XRD and DFT for complex **5** shows dramatic differences in the structures (SD) and an explanation will be given in the following sections.

3.3. Electronic ground state structures from density functional theory

We used seven different density functionals to calculate the electronic structures in the ground states of complexes **1**–**6** in DCM. For calculations with different density functionals, strong variations in the electronic structures and HOMO–LUMO gap energies have been reported in previous work by other research groups [54,59,60]. We evaluated those variations in our calculations (see SD) and found that only the hybrid functionals (B3LYP, PBE0-GD3, M06) incorporating a portion of exact exchange from Hartree–Fock (HF) theory predict HOMO–LUMO energies which are in agreement with the distinct absorption edges observed in the UV–Vis spectra of the complexes (SD and [73,74]). Based on these findings, in the following we discuss the results from calculations employing such a hybrid functional, namely PBE0-GD3.

In Fig. 5 we display the calculated electronic structure of complex **1** in DCM. Similar figures for complexes **2**–**6** can be found in

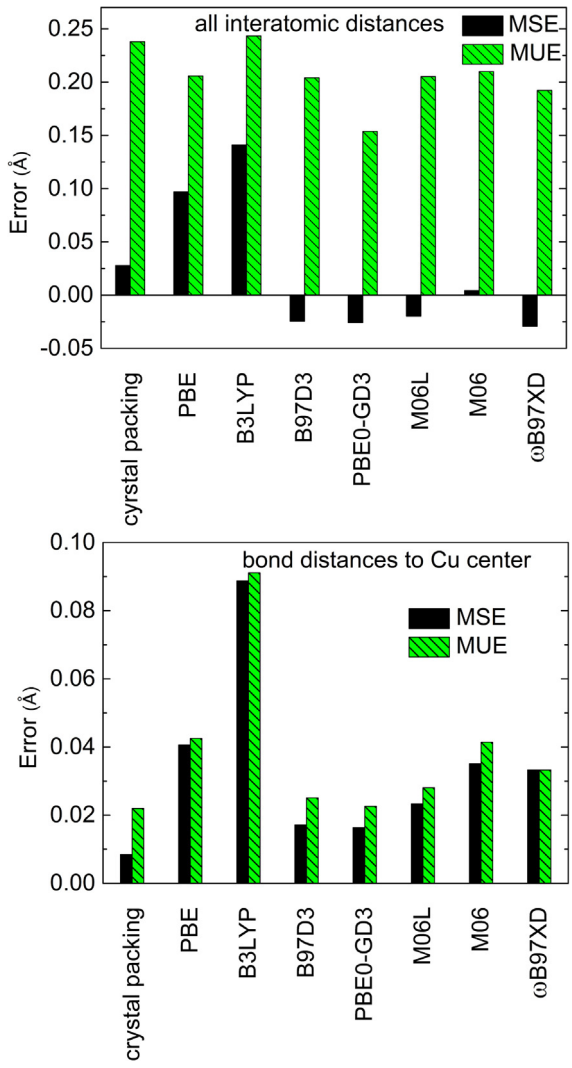

Fig. 3. Mean unsigned error (MUE) and mean signed error (MSE) for an analysis including all interatomic distances (upper graph) and only Cu-ligand bonds (lower graph) respectively. "Crystal packing" gives values for a comparison of our measured molecular structures of complexes **1**, **2** and **6** with previously reported molecular structures from XRD [44,48–50,74]. The MSE-s and MUE-s which are labeled by the designations of the functionals compare molecular structures as calculated within this work using DFT (G09 [78]) with measured molecular structures from XRD (this work and Refs. [44,45,48–50,73,74]); for complexes with multiple crystal structures the mean MUE and MSE are displayed.

the SD. To calculate the PDOS, every complex was divided into three parts: the Cu center, the DPEphos ligand and the NN ligand, and their percentage contributions were obtained as the sum of the atomic orbital coefficient squares. The nature of each molecular orbital was then assigned based on its PDOS.

We first compared results for complexes **1**–**4** and **6**, as the results for complex **5** differ significantly. For complexes **1**–**4** and **6**, we observed that the HOMO has predominant DPEphos lone pair (~55%) and Cu d_{yz} (~35%) character (axis definition SI), while the LUMO is delocalized over the NN ligands (~97%, π^* orbitals). The HOMO-1 orbitals show Cu d contributions of 35–60% and smaller π^* DPEphos, and lone pair DPEphos and NN character. This is in agreement with the DFT results by Zhang et al. [50] for complexes **1** and **2** in the gas-phase. Similar to the DFT results by Yang et al. [49], for simplified versions of complexes **1** and **2** in the gas-phase, small ligand-dependent differences in the MO composition are observed, with a slightly increasing Cu d orbital character in the HOMO and HOMO-1 in the sequence complex **1** > **2** > **3**. More dramatic variations are found for complex **4** and **6** (SD), and this is also expected considering the larger differences in their NN ligand structure. Their Cu d orbital character in the HOMO is similar to that of complex **1**, but for the HOMO-1, on the other hand, a 10% decrease of the Cu contribution is found.

In general, as expected for all complexes MOs with high contributions from the NN ligands show strong NN ligand-dependent energy changes in comparison to those with smaller NN character. In particular, for complexes **1**–**4** and **6**, the HOMOs (NN π^* character ~8%) show smaller variations in their energy (complex **1**: −6.21 eV; complex **2**: −6.18 eV; complex **3**: −6.13 eV; complex **4**: −6.25 eV; complex **6**: −6.25 eV) than the LUMOs (NN π^* character ~100%; complex **1**: −2.24 eV; complex **2**: −2.17 eV; complex **3**: −2.1 eV; complex **4**: −2.15 eV; complex **6**: −2.75 eV). The LUMO energies for complexes **2**, **3** and **4** are 0.07 eV, 0.014 eV and 0.09 eV higher in comparison to complex **1**, respectively, and the effect is not compensated by the relative change in the HOMO energies of +0.03 eV, +0.08 eV and −0.04 eV. We explain the higher LUMO energy in complexes **2**, **3** and **4** by their lower electronegativity for the N atoms of the NN ligand in comparison to complex **1**, as the electron-donating methyl, phenethyl and butyl groups in dmp, dpep and dbp push charge into the phen moiety. As a consequence, more energy is required to transfer an additional electron into the dmp, dpep and dbp ligand and the LUMO energy is enhanced. Furthermore, a combination of effects is also possible and Kuang and co-workers [44] have argued that interligand steric repulsions lead to an elongation of the Cu–P bonds in complex **2** and possibly also destabilize its CT excited state. For complex **6**,

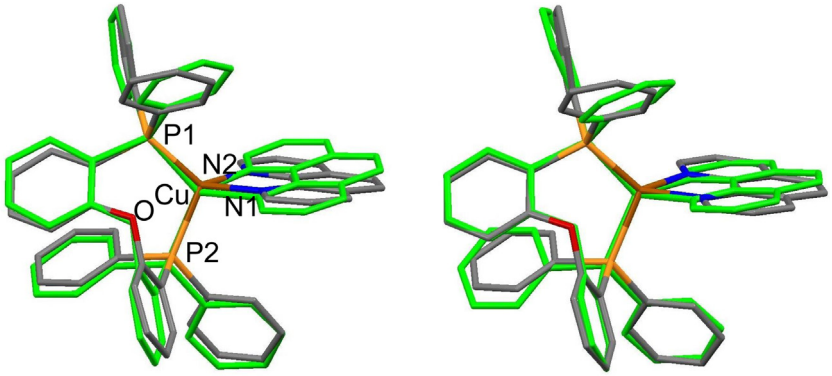

Fig. 4. Superposition of the B3LYP [80,81] **(left)** or PBE0-GD3-optimized [79,83,84] **(right)** (green) molecular ground state structure of complex **1** with the structure as derived from XRD (element-colored) [44]. The PBE0-GD3 calculated structure shows a more accurate prediction of the overall geometry from XRD experiments, in particular also for the phen moiety. (Color online.)

Table 2
Important bond lengths (Å) and angles (deg) of complexes **1**–**6** in their ground state in single crystals (Exp.) and as calculated by DFT (Calc.) for a DCM solution. Experimental data for complex **3**, **4** and **5** from Refs. [44,45,73]. It should be noted that our results for complex **1** show a disorder of the phen ligand (two positions with occupancy of 75:25; CCDC 1498327).

Complex	**1**		**2**		**3**		**4**		**5**		**6**	
	Exp.	Calc.	Exp.	Calc.	Exp. [44]	Calc.	Exp. [45]	Calc.	Exp. [73]	Calc.	Exp.	Calc.
Bond												
Cu–N(1)	2.11(1) 2.053(4)	2.111	2.094(2)	2.126	2.097(2)	2.136	2.088(3)	2.100	2.050	2.110	2.087(2)	2.095
Cu–N(2)	2.05(1) 2.078(4)	2.086	2.082(2)	2.133	2.109(2)	2.151	2.082(3)	2.103	2.083	2.080	2.075(2)	2.090
Cu–P(1)	2.1943(8)	2.247	2.262(7)	2.282	2.279(6)	2.284	2.237(8)	2.232	2.205	2.247	2.2475(8)	2.234
Cu–P(2)	2.270(1)	2.258	2.260(7)	2.268	2.271(7)	2.277	2.308(1)	2.299	2.310	2.258	2.2535(8)	2.299
Cu···O	3.182(2)	3.070	3.153(2)	3.206	3.257	3.219	3.226	3.188	3.254	3.078	3.215(2)	3.221
Angle												
N(1)–Cu–N(2)	81.0(5) 81.6(2)	80.07	81.05(8)	79.28	80.51(8)	78.80	80.90(1)	80.61	81.0(1)	79.96	78.93(9)	78.88
N(1)–Cu–P(1)	114.4(3) 123.6(1)	107.12	107.59(6)	106.23	105.44(6)	104.90	124.34(7)	123.40	121.9(1)	107.45	109.15(6)	120.29
N(1)–Cu–P(2)	99.1(3) 103.1(1)	109.57	115.23(6)	119.22	121.44(6)	123.04	100.13(7)	100.43	102.4(1)	109.35	109.35(6)	101.57
N(2)–Cu–P(1)	131.5(4) 123.1(2)	125.26	121.56(6)	118.89	121.75(6)	119.32	121.71(8)	121.82	134.9(1)	124.63	117.70(6)	126.93
N(2)–Cu–P(2)	103.5(4) 100.9(2)	112.56	110.49(6)	115.07	111.57(6)	114.72	104.58(8)	103.49	97.3(1)	113.54	114.02(6)	102.61
P(1)–Cu–P(2)	117.50(3)	115.05	115.98(3)	113.68	112.91(2)	112.39	117.98(3)	118.61	112.28(5)	114.73	119.60(3)	118.24

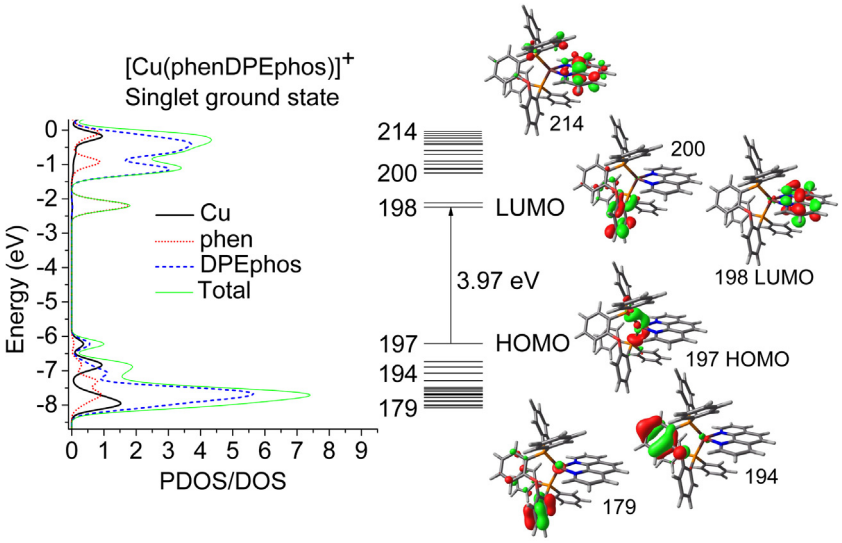

Fig. 5. Total and partial density of states and energy level diagram of the frontier molecular orbitals together with selected three-dimensional molecular orbital plots calculated with G09 [78] at the PBE0-GD3 [79,83,84] level for the ground state of complex **1** in DCM.

we suggest that its significantly lower LUMO orbital energy is a consequence of the larger conjugation and increase in delocalization for the bq ligand with respect to phen, which goes along with a smaller reduction potential for bq [99]. This behavior is in agreement with previous reports on the photophysical properties for the complexes in solution [43–45,48–50,73,74].

Results for complex **5** differ significantly with respect to complexes **1**–**4** and **6** (see also SD). The LUMO and HOMO of complex **5** show nearly identical character to the LUMO-s and HOMO-1 for complexes **1**–**4** and **6**, namely NN π^* and Cu d (35%)/DPEphos lone pair (55%) respectively. However, the HOMO of complex **5** exhibits predominately NH_2 lone pair character (95%). In other words, in comparison to complexes **1**–**4** and **6**, the introduction of an NH_2 group in **5** results in an additional MO in the HOMO–LUMO energy gap region. As a consequence of this orbital ordering, the ground and excited state properties for **5** are significantly different than those for complexes **1**–**4** and **6** (see also excited states).

3.4. Optical absorption spectra

We have calculated the energies of the first 40 lowest singlet and triplet transitions for complexes **1**–**6** using TD-DFT. The results for the selected singlet transitions are given in Table 3 and the results for the triplet transitions can be found in the SD. The character of each transition was assigned based on the character of the MO-s participating in the excitation. Transitions within a ligand are denoted as intraligand (IL) excitations, transitions from one ligand to another as ligand-to-ligand charge transfer (LLCT) excitations and transitions from the Cu center to one of the ligands as MLCT transitions.

In Fig. 6 we compare our experimental and TD-DFT calculated optical absorption spectra for complex **1** in DCM. Analogue graphs for complexes **2**–**6** can be found in the SD. There is excellent agreement between the spectra, in particular as TD-DFT tends to frequently overestimate transition energies of excitations,

Table 3
Excitation wavelength $\lambda_{calc.}$, oscillator strengths f and composition of selected TD-DFT calculated singlet excited states for the cations of complexes **1**–**6** in DCM. Experimental wavelength maxima for the respective lowest energy absorption bands are given as $\lambda_{exp.}$, they consist of several transitions. $\lambda_{exp.}$ for complex **3**, **4** and **5** from Refs. [44,45,73].

Complex	State	$\lambda_{calc.}$ (nm)	$\lambda_{exp.}$ (nm)	f	Transition	Character
1	1	396	392	0.105	HOMO → LUMO (93%)	MLCT/LLCT
1	2	374		0.016	HOMO → LUMO+1 (96%)	MLCT/LLCT
1	3	371		0.013	HOMO-1 → LUMO (71%)	MLCT/LLCT
2	1	392	382	0.084	HOMO → LUMO (95%)	MLCT/LLCT
2	2	364		0.024	HOMO → LUMO+1 (97%)	MLCT/LLCT
2	3	355		0.008	HOMO-1 → LUMO (87%)	MLCT/IL
3	1	391	378 [44]	0.074	HOMO → LUMO (95%)	MLCT/LLCT
3	2	362		0.021	HOMO → LUMO+1 (97%)	MLCT/LLCT
3	3	345		0.010	HOMO-1 → LUMO (91%)	MLCT/IL
4	1	383	380 [45]	0.074	HOMO → LUMO (97%)	MLCT/LLCT
4	2	363		0.001	HOMO-2 → LUMO (81%)	MLCT/IL
4	3	358		0.025	HOMO → LUMO +1 (93%)	MLCT/LLCT
5	1	433	383 [73]	0.050	HOMO → LUMO (99%)	IL
5	2	386		0.070	HOMO-1 → LUMO (91%)	MLCT/LLCT
5	3	368		0.019	HOMO-2 → LUMO (77%)	MLCT/LLCT/IL
6	1	463	449	0.064	HOMO → LUMO (97%)	MLCT/LLCT
6	2	432		0.001	HOMO-2 → LUMO (48%) HOMO-1 → LUMO (45%)	MLCT/LLCT/IL
6	3	404		0.015	HOMO-2 → LUMO (41%) HOMO-1 → LUMO (48%)	MLCT/LLCT/IL

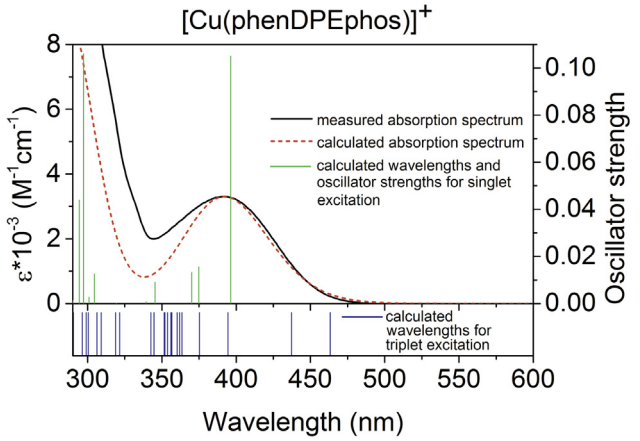

Fig. 6. Experimentally measured (black solid line) and calculated absorption spectrum (red dashed line), calculated transition wavelengths and oscillator strengths for singlet (green bars) and triplet excitation (blue bars) for complex **1** in DCM. TD-DFT transition lines were convoluted with Gaussians of FWHM 4000/cm using Gaussum 2.2. [78] and calculated extinction coefficients ε were scaled to match the experimental values. (Color online.)

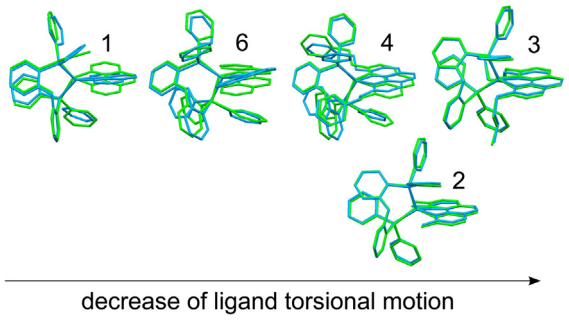

Fig. 7. Comparison of molecular structures in the lowest lying triplet excited state (blue) and in the ground state (green) of complexes **1**–**4** and **6** in DCM as calculated with G09 [78] by DFT at the PBE0-GD3 [79,83,84] level. (Color online.)

accompanied by a substantial charge density redistribution [100–103]. All the spectra show two transition band maxima in the UV–Vis region. The bands in the UV region of the experimental absorption spectra of all the complexes stem from transitions with mixed MLCT, LLCT and IL character. The experimental absorption band maxima in the blue region originate mainly from transitions at 396 nm (**1**), 392 nm (**2**), 391 nm (**3**), 383 nm (**4**), 386 nm (**5**) and 463 nm (**6**), with oscillator strengths of 0.105 (**1**), 0.084 (**2**), 0.074 (**3**), 0.074 (**4**), 0.070 (**5**) and 0.064 (**6**), and MLCT/LLCT character (HOMO → LUMO 93% (**1**), 95% (**2**), 95% (**3**), 97% (**4**), and 92% (**6**) and HOMO-1 → LUMO 91% (**5**)). Here an electron is essentially transferred from the d_{yz} orbitals at the Cu center and the lone pair orbitals of the DPEphos ligand to the π^* orbitals of the NN ligand. For complexes **1**–**4** and **6**, this excitation corresponds to the energetically lowest singlet (HOMO → LUMO) but for complex **5**, it corresponds to the second lowest singlet excitation (HOMO-1 → LUMO). The energetically lowest excitation in **5** corresponds to a HOMO → LUMO excitation (99%), where an electron is excited from the lone pair orbitals of the donating NH_2 group into the π^* orbitals of the phen moiety. This excitation shows as a low energy tail in the absorption spectrum of **5** [73] and is not seen for complexes **1**–**4** and **6**.

3.5. Relaxation of singlet excited states and triplet excited state geometric structures

We have optimized the geometric structures in the lowest triplet excited states of complexes **1**–**6** in DCM. In Fig. 7 we compare those structures with the calculated structures for the ground state, but only for complexes **1**–**4** and **6**, as complex **5** shows significantly different behavior for its lowest triplet excited state. The main difference is a substantial decrease in the dha between the N–Cu–N and P–Cu–P planes from 88.9° (**1**), 82.5° (**2**), 79.9° (**3**), 88.4° (**4**) and 89.3° (**6**) in the ground state to 58.0° (**1**), 69.7° (**2**), 67.1° (**3**), 73.0° (**4**) and 65.8° (**6**) respectively in the ^{3}CT state. This change corresponds to a ligand torisional motion, is in agreement with results for other Cu(I) complexes [21–35] and shows that the dha is an important parameter in the excited state dynamics of complexes **1**–**4** and **6**. The largest changes are observed for complexes **1** and **6**, 30° and 23° respectively, with smaller changes for complexes **4**, **2** and **3** of 15°, 13° and 13° respectively. A sterically less demanding ligand facilitates a ligand torsional motion and decrease of the dha in the excited states. This change in dha is accompanied by corresponding rotations and displacements of

the phenyl groups of the DPEphos ligand as well as changes in important bond lengths and angles (Table 4). In comparison to the ground state, the N(1)–Cu–P(1) and N(2)–Cu–P(2) angles decrease by 1–15° and N(1)–Cu–P(2) and N(2)–Cu–P(1) increase by 3–30° in the ^{3}CT states. Again, the largest differences are observed for complex **1**, the smallest for complex **3**. At the same time a shortening of all the Cu–N bonds and an elongation of all the Cu–P bonds by ~0.11 Å and an increase in the Cu···O distance by on average 0.05 Å is observed in the ^{3}CT state, similar to the trend reported for other Cu(I) complexes with phosphine ligands [51]. The N–Cu–N angles increase from ~79° to ~84°, while the P–Cu–P angles decrease from ~115° to ~105°. The natural bite angle of DPEphos is around ~102°, with values as high as ~120° [104]. In the ^{3}CT state the structure of the DPEphos ligand relaxes in the direction of its natural bite angle, while the Cu–N distances becomes shorter, leading to steric stress and a displacement of the NN ligand structure from its natural bite angle around ~80°. This is reflected in the C(N)–C(N) bond lengths which are shortened by ~0.04 Å and the N–C bonds which are elongated by 0.01–0.05 Å in the triplet excited state.

In addition to the molecular structure for the ^{3}CT state, for comparison, the structure in the ^{1}CT state after initial phototexcitation and relaxation was also calculated, but only for complex **2** because TD-DFT calculations of excited state properties typically require significantly more computational effort than DFT calculations. The structural parameters such as the dha between the N–Cu–N and P–Cu–P planes and molecular geometries (SD) including bond lengths and angles are nearly identical for the two states. We conclude that a ligand torsional motion in the ^{1}CT state of complex **2** results in a molecular geometry in the minimum of the ^{1}CT state potential energy surface which is nearly identical to that in the ^{3}CT state.

As mentioned at the beginning of this section, the geometrical structure of complex **5** in its lowest triplet excited state is significantly different than that of complexes **1**–**4** and **6**, and this is a consequence of the IL nature of the lowest singlet excitation in **5**. This difference is also reflected in deviations of the bonding distances and valence angles between the ground and lowest triplet excited state of **5** (Table 4). Moreover, it should be noted that the calculated molecular structure in the lowest triplet excited state of complex **5** shows excellent agreement with the molecular structure derived from ground state XRD [73] (SD). The molecular structure in the crystal is best represented by the geometry of an IL state where lone pair electrons of the NH_2 group are transferred to the phen moeity.

3.6. Electronic structure of the triplet excited state

We analyzed the electronic structures for complexes **1**–**6** in their lowest triplet excited states. Mulliken charges arising from a Mulliken population analysis [108] for complexes **1**–**4** and **6** point at the difference between the ground state and the lowest triplet excited state being of MLCT/LLCT nature. The Cu atom and the DPEphos ligand become more positive in the triplet state by ~0.20–0.25 e and ~0.30–0.35 e respectively and the NN ligands gain in total around 0.55 e for all the complexes. In contrast, the Mulliken charges for the ground and lowest triplet excited state of complex **5** indicate no significant changes for the Cu atom and the DPEphos ligand. However, the NH_2 and phen moeity become more positive and negative respectively by around 0.17 e in the

Table 4
The important bond lengths (Å) and angles (deg) of complexes **1**–**6** in the lowest lying triplet excited state as calculated by DFT. Bond and angle labeling according to atom labels for compound **1**–**6** (Fig. 2; SD).

Bond	1	2	3	4	5	6	Angle	1	2	3	4	5	6
Cu–N(1)	1.978	1.968	1.974	1.990	2.096	1.987	N(1)–Cu–N(2)	84.07	84.09	84.03	84.40	80.34	83.06
Cu–N(2)	1.984	2.038	2.047	2.000	2.098	1.998	N(1)–Cu–P(1)	100.70	99.85	99.17	112.24	125.28	105.30
Cu–P(1)	2.341	2.381	2.381	2.366	2.216	2.361	N(1)–Cu–P(2)	136.99	133.45	136.61	124.45	101.60	129.70
Cu–P(2)	2.354	2.362	2.383	2.380	2.313	2.380	N(2)–Cu–P(1)	138.16	124.57	126.00	128.64	131.76	134.23
Cu ··O	3.100	3.280	3.325	3.228	3.343	3.273	N(2)–Cu–P(2)	99.99	110.08	109.22	101.25	96.62	101.73
							P(1)–Cu–P(2)	103.69	106.21	104.47	106.23	113.55	105.80

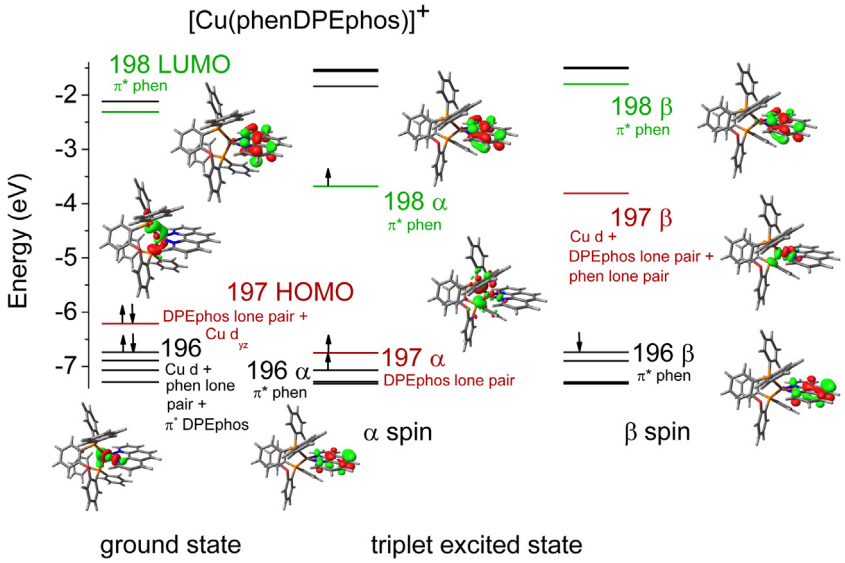

Fig. 8. Comparison of the energy level diagram of the frontier molecular orbitals together with selected three-dimensional molecular orbital plots calculated with G09 [78] at the PBE0-GD3 [79,83,84] level for the ground and lowest lying triplet excited state of complex **1** in DCM.

triplet excited state, again showing the phen* IL character of this state. Energies for the ^{3}CT states of complexes **1**–**4** and **6** in DCM are 2.15, 2.36, 2.39, 2.48 and 1.81 eV higher than for their ground state respectively. The trend of decreasing energy differences in the order complex **4 > 3 > 2 > 1** maps the trend for the experimental emission energies (SI and [44,45,48–50]; emission maxima: 544 (**4**), 560 (**3**), 565 (**2**) and 700 nm (**1**)). A larger geometrical relaxation in the excited states of complex **1** results in a larger decrease in energy for these states in comparison to complexes **2**–**4**. Following the energy gap law, this larger decrease in energy should correspond to a significantly lower lifetime of the ^{3}CT state of **1** and indeed this has been observed previously (τ = 0.2 (**1**), 14.3 (**2**) and 16.1 μs (**3**)) [44]. A comparison between complexes **4** and **6** does not provide significant insight as the energy gap law works best for complexes with a good similarity of structure [105].

In Fig. 8 we compare the results for the energy-level diagrams, MOs and orbital compositions from our DFT calculations for the triplet excited and the ground state of complex **1** in DCM. As for any unrestricted calculations, there are two complete sets of orbitals, one for the α electrons (α spin) and one for the β electrons (β spin) which use the same set of basis functions but different molecular orbital coefficients. For complexes **1**–**4** and **6** in the flattened ^{3}CT state the former ground state HOMO orbitals and orbitals just below gain significant DPEphos and NN character, both from lone pair and π^* orbitals. In particular, the NN π^* orbital character is enhanced while the contribution of the Cu center decreases significantly. In contrast, the former ground state LUMO and LUMO+1 orbitals still show predominant NN π^* character in the ^{3}CT state. For complex **5** in the lowest triplet excited state, the former ground state HOMO orbitals gain significant Cu d, DPEphos (lone pair) and NN π^* character, but the former ground state LUMO orbitals exhibit still mainly NN π^* character.

4. Conclusions

We have studied the electronic and geometric structures in the ground and ^{3}CT states of six phosphorescent heteroleptic [Cu(NN)(DPEphos)]$^+$ complexes with varying NN ligand structures using DFT. The soundness of the calculations has been verified by ground state validation studies. We compared the ability of seven density functionals to predict the molecular ground state geometries and absorption spectra derived from single-crystal XRD and solution-phase UV–Vis absorption spectroscopy respectively. Our analysis shows that the methods which account for dispersion predict the geometrical structures of the molecules more accurately than standard approaches which do not consider dispersion. The latter systematically overestimate the internuclear distances and give expanded molecular structures. Moreover, the experimental absorption energies are only modeled accurately in calculations with hybrid functionals which incorporate a portion of exact exchange from HF theory.

Results from the DFT calculations at the PBE0-GD3 level are in good agreement with the experimental data. They explain deviations in the molecular geometries, optical absorption spectra as well as excited state emission quantum yields and lifetimes for complexes with different NN ligand structures through differences in the electronegativity, conjugation and bulkiness of those ligands. In particular, in comparison to the ground state, the results show a decrease of the dihedral angle between the N–Cu–N and P–Cu–P planes for the ^{3}CT excited states with MCLT/LLCT character. Sterically more demanding ligands impede this change in geometry. In this context, it would be important to investigate the dynamics in the excited states of [Cu(NN)(DPEphos)]$^+$ complexes, for example in time-resolved experiments, and here we expect that the current results will significantly facilitate the interpretation of data.

Acknowledgements

We thank R.W. Hartsock and K.J. Gaffney for discussion and for access to the Gaffney group chemistry lab at the PULSE Institute of the SLAC National Accelerator Laboratory (Stanford University, Stanford, California 94305, USA). Furthermore, we thank J. Bienert at the Facility for Synthetic Chemistry at the Max Planck Institute for Biophysical Chemistry (Göttingen, Germany) for the chemcial analysis of the synthesized Cu(I) complexes. Moreover, we thank V. Mäckel and L. Glaser for detailed discussion of the manuscript. K.K. acknowledges financial support from the Volkswagen Foundation under the Peter Paul Ewald fellowship program (87008) and from SFB 755 (BO3). S.T. acknowledges additional support from SFB 1073 (BO6).

Appendix A. Supplementary data

CCDC 1498327–1498329 contains the supplementary crystallographic data for complexes **1**, **2** and **6**. These data can be obtained free of charge via http://www.ccdc.cam.ac.uk/conts/retrieving.html, or from the Cambridge Crystallographic Data Centre, 12 Union Road, Cambridge CB2 1EZ, UK; fax: (+44) 1223-336-033; or e-mail: deposit@ccdc.cam.ac.uk. Supplementary data associated with this article can be found, in the online version, at http://dx.doi.org/10.1016/j.poly.2016.12.035.

References

[1] B. O'Regan, M. Grätzel, Nature 353 (1991) 737.
[2] M.K. Nazeeruddin, M. Grätzel, Struct. Bond 123 (2007) 113.
[3] N.A. Rakow, K.S. Suslick, Nature 406 (2000) 710.
[4] B.A. DeGraff, J.N. Demas, Coord. Chem. Rev. 211 (2001) 317.
[5] V.W.-W. Yam, K.M.-C. Wong, Chem. Commun. 47 (2011) 11579.
[6] M. Elliott, F. Pichot, C.J. Bloom, L.S. Rider, J. Am. Chem. Soc. 120 (1998) 6781.
[7] H. Yersin, A.F. Rausch, R. Czerwieniec, T. Hofbeck, T. Fischer, Coord. Chem. Rev. 255 (2011) 2622.
[8] V. Balzani, S. Campagna (Eds.), Photochemistry and Photophysics of Coordination Compounds I, Springer, Berlin Heidelberg, Berlin, Heidelberg, 2007.
[9] V. Balzani, S. Campagna (Eds.), Photochemistry and Photophysics of Coordination Compounds II, Springer, Berlin Heidelberg, Berlin, Heidelberg, 2007.
[10] W. Zhang, R. Alonso-Mori, U. Bergmann, C. Bressler, M. Chollet, A. Galler, W. Gawelda, R.G. Hast, R.W. Hartsock, T. Kroll, K.S. Kjær, K. Kubiček, H.T. Lemke, H.W. Liang, D.A. Meyer, M.M. Nielsen, C. Purser, J.S. Robinson, E.I. Solomon, Z. Sun, D. Sokaras, T.B. van Driel, G. Vankó, T.-C. Weng, D. Zhu, K.J. Gaffney, Nature 509 (2014) 345.
[11] N. Armaroli, Chem. Soc. Rev. 30 (2001) 113.
[12] N. Armaroli, G. Accorsi, F. Cardinali, A. Listorti, Top. Curr. Chem. 280 (2007) 69.
[13] R. Kia, V. Mirkhani, S. Harkema, G.J. van Hummel, Inorg. Chim. Acta 360 (2007) 3369.
[14] R. Kia, M. Scholz, P.R. Raithby, S. Techert, Inorg. Chim. Acta 423 (2014) 348.
[15] P.C. Ford, Rev. Chem. Intermed. 2 (1979) 267.
[16] A. Juris, V. Balzani, F. Barigelletti, S. Campagna, P. Belser, A. von Zelewsky, Coord. Chem. Rev. 84 (1988) 85.
[17] R.D. Costa, E. Ort, H.J. Bolink, F. Monti, G. Accorsi, N. Armaroli, Angew. Chem., Int. Ed. 51 (2012) 8178.
[18] M.W. Mara, K.A. Fransted, L.X. Chen, Coord. Chem. Rev. 282 (2015) 2.
[19] W. Zhang, K.S. Kjær, R. Alonso-Mori, U. Bergmann, M. Chollet, L.A. Fredin, R.G. Hadt, R.W. Hartsock, T. Harlang, T. Kroll, et al., Chem. Sci. 8 (2017) 515.
[20] M. Jäger, L. Freitag, L. González, Coord, Chem Rev. 304–305 (2015) 146.
[21] L.X. Chen, G. Jennings, T. Liu, D.J. Gosztola, J.P. Hessler, D.V. Scaltrito, G.J. Meyer, J. Am. Chem. Soc. 124 (2002) 10861.
[22] Z.A. Siddique, Y. Yamamoto, T. Ohno, K. Nozaki, Inorg. Chem. 42 (2003) 6366.
[23] M.Z. Zgierski, J. Chem. Phys. 118 (2003) 4045.
[24] L.X. Chen, G.B. Shaw, I. Novozhilova, T. Liu, G. Jennings, K. Attenkofer, G.J. Meyer, P. Coppens, J. Am. Chem. Soc. 125 (2003) 7022.
[25] G.B. Shaw, C.D. Grant, H. Shirota, E.W. Castner Jr., G.J. Meyer, L.X. Chen, J. Am. Chem. Soc. 129 (2007) 2147.
[26] M. Iwamura, S. Takeuchi, T. Tahara, J. Am. Chem. Soc. 129 (2007) 5248.
[27] J.V. Lockard, S. Kabehie, J.I. Zink, G. Smolentsev, A. Soldatov, L.X. Chen, J. Phys. Chem. B 114 (2010) 14521.

[28] M. Iwamura, H. Watanabe, K. Ishii, S. Takeuchi, T. Tahara, J. Am. Chem. Soc. 133 (2011) 7728.
[29] N.A. Gothard, M.W. Mara, J. Huang, J.M. Szarko, B. Rolczynski, J.V. Lockhard, L. X. Chen, J. Phys. Chem. A 116 (2012) 1984.
[30] T.J. Penfold, S. Karlsson, G. Capano, F.A. Lima, J. Rittmann, M. Reinhard, M.H. Rittmann-Frank, O. Braem, E. Baranoff, R. Abela, I. Tavernelli, U. Rothlisberger, C.J. Milne, M. Chergui, J. Phys. Chem. A 117 (2013) 4591.
[31] M.W. Mara, N.E. Jackson, J. Huang, A.B. Stickrath, X. Zhang, N.A. Gothard, M.A. Ratner, L.X. Chen, J. Phys. Chem. B 117 (2013) 1921.
[32] M. Tromp, A.J. Dent, J. Headspith, T.L. Easun, X.Z. Sun, M.W. George, O. Mathon, G. Smolentsev, M.L. Hamilton, J. Evans, J. Phys. Chem. B 117 (2013) 7381.
[33] M. Iwamura, S. Takeuchi, T. Tahara, Phys. Chem. Chem. Phys. 16 (2014) 4143.
[34] L. Hua, M. Iwamura, S. Takeuchi, T. Tahara, Phys. Chem. Chem. Phys. 17 (2015) 2067.
[35] S. Garakyaraghi, E.O. Danilov, C.E. McCusker, F.N. Castellano, J. Phys. Chem. A 119 (2015) 3181.
[36] M.W. Blaskie, D.R. McMillin, Inorg. Chem. 19 (1980) 3519.
[37] J.R. Kirchhoff, R.E. Gamache, M.W. Blaskie, A.A. del Paggio, R.K. Lengel, D.R. McMillin, Inorg. Chem. 22 (1983) 2380.
[38] C.E.A. Palmer, D.R. McMillin, C. Kirmaier, D. Holten, Inorg. Chem. 26 (1987) 3167.
[39] D.R. McMillin, K.M. McNett, Chem. Rev. 98 (1998) 1201.
[40] D.V. Scaltrito, D.W. Thompson, J.A. O'Callaghan, G.J. Meyer, Coord. Chem. Rev. 208 (2000) 243.
[41] M.K. Eggleston, D.R. McMillin, K.S. Koenig, A.J. Pallenberg, Inorg. Chem. 36 (1997) 172.
[42] C.T. Cunningham, K.L.H. Cunningham, J.F. Michalec, D.R. McMillin, Inorg. Chem. 38 (1999) 4388.
[43] D.G. Cuttell, S.-M. Kuang, P.E. Fanwick, D.R. McMillin, R.A. Walton, J. Am. Chem. Soc. 124 (2002) 6.
[44] S.-M. Kuang, D.G. Cuttell, D.R. McMillin, P.E. Fanwick, R.A. Walton, Inorg. Chem. 41 (2002) 3313.
[45] N. Armaroli, G. Accorsi, M. Holler, O. Moudam, J.F. Nierengarten, Z. Zhou, R.T. Wegh, R. Welter, Adv. Mater. 18 (2006) 1313.
[46] Q. Zhang, Q. Zhou, Y. Cheng, L. Wang, D. Ma, X. Jing, F. Wang, Adv. Funct. Mater. 16 (2006) 1203.
[47] F. Dumur, Org. Electron. 21 (2015) 27.
[48] R.D. Costa, D. Tordera, E. Ortí, H.J. Bolink, J. Schönle, S. Graber, C.E. Housecroft, E.C. Constable, J.A. Zampese, J. Mater. Chem. 21 (2011) 16108.
[49] L. Yang, J.-K. Feng, A.-M. Ren, M. Zhang, Y.-G. Ma, X.-D. Liu, Eur. J. Inorg. Chem. 10 (2005) 1867.
[50] K. Zhang, D. Zhang, Spec. Acta Part A 124 (2014) 341.
[51] I.I. Vorontsov, T. Graber, A.J. Kovalevsky, I.V. Novozhilova, M. Gembicky, Y.-S. Chen, P. Coppens, J. Am. Chem. Soc. 131 (2009) 6566.
[52] S. Tschierlei, M. Karnahl, N. Rockstroh, H. Junge, M. Beller, S. Lochbrunner, ChemPhysChem 15 (2014) 3709.
[53] Y. Minenkov, A. Singstad, G. Occhipinti, V.R. Jensen, Dalton Trans. 41 (2012) 5526.
[54] J. Kreutzer, P. Blaha, U. Schubert, Comput. Theor. Chem. 1084 (2016) 162.
[55] F. Neese, W. Ames, G. Christian, M. Kampa, D.G. Liakos, D.A. Pantazis, M. Roemelt, P. Surawatanawong, S.F. Ye, Adv. Inorg. Chem. 62 (2010) 301.
[56] H. Schwarz, Angew. Chem., Int. Ed. 42 (2003) 4442.
[57] A.J. Cohen, P. Mori-Sanchez, W.T. Yang, Science 321 (2008) 792.
[58] C.J. Cramer, D.G. Truhlar, Phys. Chem. Chem. Phys. 11 (2009) 10757.
[59] J. Muscat, A. Wander, N.M. Harrison, Chem. Phys. Lett. 342 (2001) 397.
[60] S. Tretiak, K. Igumenschev, V. Chernyak, Phys. Rev. B 71 (2005) 33201.
[61] M. Bühl, H.J. Kabrede, Chem. Theor. Comput. 2 (2006) 1282.
[62] K.E. Riley, K.M. Merz, J. Phys. Chem. A 111 (2007) 6044.
[63] M. Bühl, C. Reimann, D.A. Pantazis, T. Bredow, F.J. Neese, Chem. Theor. Comput. 4 (2008) 1449.
[64] N. Sieffert, M. Bühl, Inorg. Chem. 48 (2009) 4622.
[65] P. Rydberg, L. Olsen, J. Phys. Chem. A 113 (2009) 11949.
[66] J. Yuan, R.P. Hughes, J.A. Golen, A.L. Rheingold, Organometallics 29 (2010) 1942.
[67] N. Marom, A. Tkatchenko, M. Scheffler, L. Kronik, J. Chem. Theory Comput. 6 (2010) 81.
[68] C.A. Jimenez-Hoyos, B.G. Janesko, G.E. Scuseria, J. Phys. Chem. A 113 (2009) 11742.
[69] T.A. Mohamed, I.A. Shaaban, R.S. Farag, W.M. Zoghaib, M.S. Afifi, Spec. Acta Part A 135 (2015) 417.
[70] J.J. Sardrooni, A. Rastkar, N.R. Yousefina, J. Azamat, J. Theor. Comput. Chem. 12 (2013) 1350066.
[71] S. Kristyan, P. Pulay, Chem. Phys. Lett. 229 (1994) 175.
[72] J.R. Reimers, Z.-L. Cai, A. Bilic, N.S. Hush, Ann. N. Y. Acad. Sci. 1006 (2003) 235.
[73] X.-X. Yao, Y.-M. Guo, R. Liu, X.-Y. Feng, H.-H. Li, N. Liu, F.-L. Yang, X.-L. Li, Polyhedron 92 (2015) 84.
[74] Q. Zhang, J. Ding, Y. Cheng, L. Wang, Z. Xie, X. Jing, F. Wang, Adv. Funct. Mater. 17 (2007) 2983.
[75] C.R. Groom, I.J. Bruno, M.P. Lightfoot, S.C. Ward, Acta Cryst. B72 (2016) 171.
[76] S. Thekku-Veedu, D. Raiser, R. Kia, M. Scholz, S. Techert, J. Phys. Chem. B 118 (2014) 3291.
[77] J. Hallmann, S. Techert, J. Phys. Chem. Lett. 1 (2010) 959.
[78] M.J. Frisch, G.W. Trucks, H.B. Schlegel, G.E. Scuseria, M.A. Robb, J.R. Cheeseman, G. Scalmani, V. Barone, B. Mennucci, G.A. Petersson, H. Nakatsuji, M. Caricato, X. Li, H.P. Hratchian, A.F. Izmaylov, J. Bloino, G. Zheng, J.L. Sonnenberg, M. Hada, M. Ehara, K. Toyota, R. Fukuda, J. Hasegawa, M. Ishida, T. Nakajima, Y. Honda, O. Kitao, H. Nakai, T. Vreven, J.A. Montgomery Jr., J.E. Peralta, F. Ogliaro, M. Bearpark, J.J. Heyd, E. Brothers, K. N. Kudin, V.N. Staroverov, T. Keith, R. Kobayashi, J. Normand, K. Raghavachari, A. Rendell, J.C. Burant, S.S. Iyengar, J. Tomasi, M. Cossi, N. Rega, J.M. Millam, M. Klene, J.E. Knox, J.B. Cross, V. Bakken, C. Adamo, J. Jaramillo, R. Gomperts, R.E. Stratmann, O. Yazyev, A.J. Austin, R. Cammi, C. Pomelli, J.W. Ochterski, R.L. Martin, K. Morokuma, V.G. Zakrzewski, G.A. Voth, P. Salvador, J.J. Dannenberg, S. Dapprich, A.D. Daniels, O. Farkas, J.B. Foresman, J.V. Ortiz, J. Cioslowski, D.J. Fox, Gaussian 09, Revision E.01, Gaussian Inc., Wallingford CT, 2013.
[79] J.P. Perdew, K. Burke, M. Ernzerhof, Phys. Rev. Lett. 77 (1996) 3865.
[80] A.D. Becke, J. Chem. Phys. 98 (1993) 5648.
[81] C. Lee, W. Yang, R.G. Parr, Phys. Rev. B 37 (1988) 785.
[82] S. Grimme, S. Ehrlich, L. Goerigk, *J. Comp. Chem.* 32 (2011) 1456.
[83] J.P. Perdew, K. Burke, M. Ernzerhof, Phys. Rev. Lett. 78 (1997) 1396.
[84] S. Grimme, J. Antony, S. Ehrlich, H. Krieg, J. Chem. Phys. 132 (2010) 154104.
[85] J.D. Chai, M. Head-Gordon, Phys. Chem. Chem. Phys. 10 (2008) 6615.
[86] J.-D. Chai, M. Head-Gordon, J. Chem. Phys. 128 (2008) 084106.
[87] Y. Zhao, D.G. Truhlar, Theor. Chem. Acc. 120 (2008) 215.
[88] Y. Zhao, Y.; Truhlar, D.G, Acc. Chem. Res. 41 (2008) 157.
[89] D. Andrae, U. Haußermann, M. Dolg, H. Stoll, H. Preuß, Theor. Chim. Acta 77 (1990) 123.
[90] R.E. Stratmann, G.E. Scuseria, M.J. Frisch, J. Chem. Phys. 109 (1998) 8218.
[91] V. Barone, M. Cossi, J. Phys. Chem. A 102 (1998) 1995.
[92] M. Cossi, V. Barone, J. Chem. Phys. 115 (2001) 4708.
[93] M. Cossi, N. Rega, G. Scalmani, V. Barone, J. Comput. Chem. 24 (2003) 669.
[94] N.M. O'Boyle, A.L. Tenderholt, K.M. Langner, *J. Comp. Chem.* 29 (2008) 839.
[95] C.F. Macrae, P.R. Edgington, P. McCabe, E. Pidcock, G.P. Shields, R. Taylor, M. Towler, J. van de Streek, J. Appl. Crystallogr. 39 (2006) 453.
[96] M.D. Hanwell, D.E. Curtis, D.C. Lonie, T. Vandermeersch, E. Zurek, G.R. Hutchison, J. Cheminform. 4 (2012) 17.
[97] http://www.chemcraftprog.com.
[98] A. Martin, A.G. Orpen, J. Am. Chem. Soc. 118 (1996) 1464.
[99] Yang, University of North Texas, Denton, Texas, 1995, PhD thesis.
[100] A. Dreuw, J.L. Weisman, M. Head-Gordon, J. Chem. Phys. 119 (2003) 2943.
[101] T.A. Niehaus, T. Hofbeck, H. Yersin, RSC Adv. 5 (2015) 63318.
[102] S. Záliš, N.B. Amor, C. Daniel, Inorg. Chem. 43 (2004) 7978.
[103] M. Turki, C. Daniel, S. Záliš, A. Vlček Jr., J. van Slageren, D.J. Stufkens, J. Am. Chem. Soc. 123 (2001) 11431.
[104] P. Dierkes, P.W.N.M. van Leeuwen, J. Chem. Soc., Dalton Trans. (1999) 1519.
[105] J.R. Lakowicz, Principles of Fluorescence Spectroscopy, Springer, New York, 2006.
[106] D. Raiser, D. Storozhuk, S. Thekku Veedu, S. Techert, Acta Cryst. A71 (2015) s484.
[107] S. Grimme, J. Comp. Chem. 27 (2006) 1787.
[108] R.S. Mulliken, J. Chem. Phys. 23 (1995) 1833.